# Physics-Informed Deep Learning for Traffic State Estimation: Illustrations With LWR and CTM Models

## ARCHIE J. HUANG [ID] AND SHAURYA AGARWAL [ID] (Senior Member, IEEE)

Civil, Environmental and Construction Engineering Department, University of Central Florida, Orlando, FL 32816, USA

CORRESPONDING AUTHOR: A. J. HUANG (e-mail: jihenghuang@knights.ucf.edu)

**ABSTRACT** We present a physics-informed deep learning (PIDL) approach to tackle the challenge of data sparsity and sensor noise in traffic state estimation (TSE). PIDL strengthens a deep learning (DL) neural network with the knowledge of traffic flow theory to accurately estimate traffic conditions. The 'physics'—a priori information of the system—acts as a regularization agent during training. We illustrate the implementation of the proposed approach with two commonly used models representing traffic physics: Lighthill-Whitham-Richards (LWR) model and the cell transmission model (CTM). The LWR implementation is illustrated with Greenshields' and inverse-lambda fundamental diagrams; whereas, CTM model implementation works with any fundamental diagram of choice. Two case studies validate the approach by reconstructing the velocity-field. Case study-I uses synthetic data generated to resemble the trajectory of connected and autonomous vehicles as captured by roadside units. Case study-II employs NGSIM data mimicking scant probe vehicle observations. We observe that the proposed PIDL approach is particularly better in state estimation with a lower amount of training data, illustrating the capability of PIDL in making precise and timely TSE even with sparse input. E.g., With 10% CAV penetration rate and a 15% added-noise, relative error for PIDL was at 22.9% compared to 30.8% for DL.

**INDEX TERMS** Physics informed deep learning, traffic state estimation, LWR model, CTM model, TSE, PIDL, PINN.

## I. INTRODUCTION

MACROSCOPIC traffic state variables, such as flow rate $f$, mean speed $v$, and vehicle density $\rho$, denote the traffic conditions on the road infrastructures in a traffic network. Through these measurements, urban planners and policymakers can perceive the congestion levels, understand traffic demand, and even recognize gridlocks and bottlenecks of a road network [1]. For example, a sharp deterioration in travel speed at a road section can indicate particular events such as traffic incidents or disturbances.

Nevertheless, these crucial measurements necessitated for traffic management and planning are oftentimes scanty and likely noisy [2]. Due to the various factors such as cost of sensor installation, the precision of vehicle detection methods, and constraints on data storage and communication, these traffic state variables are frequently observed partially [3], [4]. For instance, traffic data would only be registered at chosen locations with the scattered deployment of vehicle detectors on a highway system [5]. Additionally, this type of recorded data is often compromised with various levels of imprecision due to the presence of measurement noise in detection and sensing devices [6]. Moreover, the data collected are routinely aggregated, worsening the temporal resolution of these measurements [7], [8].

**What is TSE?** Based on the above discussion, the challenge is how to efficiently utilize limited, sparsely sampled (in spatial and temporal domains), and potentially noisy data to gain a clear sense of traffic conditions in real-time. Tools that fill the voids in traffic measurements and provide a reliable description of traffic conditions are referred to as traffic state estimation (TSE) techniques. In other

The review of this article was arranged by Associate Editor Jia Hu.

words, TSE relates to the inference of traffic state variables of road segments using partially observed traffic data [9]. Accurate and prompt TSE is of the essence for effective traffic management since control strategies are implemented accordingly [10]. For instance, the usage of ramp control on freeways exemplifies the value of TSE. It uses the measured traffic flow data to estimate freeway traffic conditions, then alternates the traffic signals to allow vehicles at the ramp into the traffic stream according to the upstream and downstream flow levels [11].

*TSE Approaches in Literature:* Given the impediment discussed above in the traffic data collection and the importance of TSE applications in transportation planning, practitioners and researchers often use a priori knowledge to estimate traffic states. These estimation procedures can be categorized as model-driven approaches and data-driven approaches, based on the type of a priori assumption they rely on [9].

**Model-driven approaches** deploy a model from the traffic flow theory in predicting traffic states. Models such as cell transmission model (CTM) [12], and switching mode model (SMM) [13] have been proposed to represent traffic flows. Lighthill-Whitham-Richards (LWR) model, along with higher-order models such as Payne-Whitham (PW) model [14], [15], Aw-Rascle-Zhang (ARZ) model [16], [17] are widely used because of their accurate traffic characterization and fair computation cost.

Kalman filter [18], and its various extensions [19]–[21] are commonly used to solve the task of TSE efficiently and calibrate the traffic flow models. The Kalman filter and its variations determine the most presumable state for the observed data, system variables of the model, and noises [9]. However, a few major challenges remain in the model-driven approach for TSE. The estimation of model parameters, changing road conditions (e.g., due to lane closures, road construction projects), and suitability of a chosen model for the exact road location of interest remain major hurdles in adopting the traffic flow model approach for TSE.

Suppose the selected traffic flow model can convincingly capture the relationship between traffic state variables such as flow and density observed in reality. In that case, the model-driven approach—based on the physics of traffic flow—can precisely predict the traffic states in unobserved areas with no data collection devices. In addition, it can yield a higher spatial and temporal resolution of traffic state data at locations where data collection technology is deployed. On the other hand, the dependence on the traffic flow model brings the vulnerability of unfit model adoption. Using standard traffic flow models with empirical evidence somewhat lowers this kind of risk. Nevertheless, the robustness of estimation in the event of an anomaly such as a traffic accident or inclement weather condition leaves room for improvement in the estimation result.

*Data-Driven Approaches:* With the advancement of statistical tools and machine learning, data-driven methods have become another type of prominent approach for TSE. Data-driven TSE adopts the insights of historically
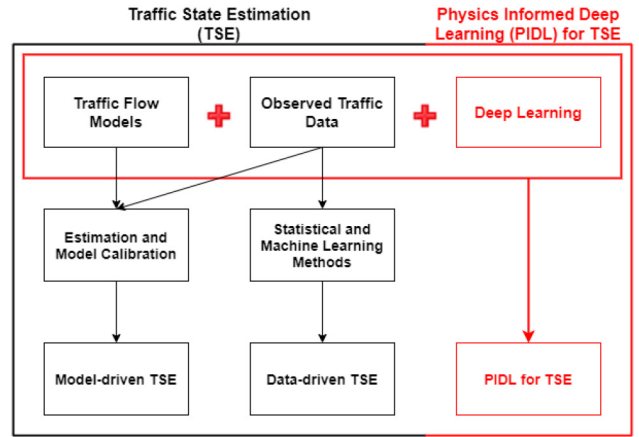


**FIGURE 1.** Traffic State Estimation Approaches.

observed traffic data for estimation and prediction tasks. It enables the model to discover the underlying traffic data structure, eliminating the requirement of fitting a traffic flow model suitable for each road segment involved. In this kind of approach, probabilistic principal component analysis [22], k-nearest neighbors [23], Deep learning [24], recurrent neural network (RNN) [25], [26] and long short-term memory (LSTM) [27], [28] neural network have all been experimented and applied in the literature.

However, the current machine learning (ML) based approaches rely overly on the obtained traffic data, which leads to *over-fitting* when applied in a different traffic scenario. The lack of robustness limits the applications of the experimental ML models. For instance, the probabilistic approach cannot distinguish some temporal patterns from long-term trends [22], and k-nearest neighbors may not be an ideal approach when unusual traffic patterns occur [23].

State-of-the-art approaches such as LSTM and RNN-type neural networks have given impressive performance in capturing the nonlinear relationships among traffic states [29]. However, LSTM and RNNs are known for the hindrance in the training process as updating the weights, and bias parameters consume immense memory and computational resources. In other words, these algorithms and their variants are not suitable for hardware acceleration. Moreover, these algorithms are affected by different random weight initialization and are also prone to over-fitting.The relationship between the conventional TSE approaches and the proposed PIDL approach is shown in Fig. 1.

*Research Questions:* Carefully analyzing the literature discussed above leads to the following two motivating research questions for this study:

1) Instead of blindly feeding the data into a learning model, can the fundamental principles of traffic flow theory be harnessed to augment the power of machine learning?

2) Can the physical laws and constraints of traffic flow in help uncover the implicit relationship between traffic state variables buried in the data?

The approach combining the advantage of machine learning and the knowledge of governing physical equations of traffic flow is termed as physics-informed deep learning (PIDL). Together, the data-driven approach and the physics of traffic flow have the potential to build a fast, resilient, and computation-friendly TSE strategy. Moreover, when the measurements of traffic states at fixed locations are unavailable due to the malfunction of sensing devices or incidents like cyber-attacks, the PIDL approach presents an ideal alternative in utilizing potentially sparse and noisy data to estimate and predict traffic state variables.

*Key Features and Contributions:* This paper offers details of the proposed PIDL algorithm by demonstrating its application using the hydrodynamic traffic conservation law (LWR) model and a numerically more appropriate discrete cell transmission (CTM) model. Two case studies are presented to evaluate the proposed methodology. The first case study uses synthetic data resembling the trajectories of connected and autonomous vehicles (CAVs) as captured by roadside units (RSUs). The second case study is designed to resemble scant observations from probe vehicles using the trajectory information from Next Generation Simulation (NGSIM) data. We investigate the accuracy and convergence-time of PIDL and a similarly configured deep learning neural network with varying levels of scantily collected traffic observations. The novel *contributions* of this paper are as follows:

1) We propose a novel physics-informed deep learning approach for traffic state estimation and reconstruction. It equips a deep learning neural network with the physics of traffic flow theory, termed as *physics informed deep learning* (PIDL).

2) We not only consider the conservation law of traffic flow in the form of the Lighthill-Whitham-Richards (LWR) model but also formulate the physics cost (loss function) using a more realistic cell transmission model (CTM). To the best of our knowledge, this is the first attempt at incorporating CTM in the training of neural networks for traffic state estimation and prediction.

3) We demonstrate the incorporation of various fundamental diagrams - Greenshields', Daganzo's, and inverse-lambda.

*Note:* This research paper is an extension of our previous conference paper [30], with significant additions. Previous work only considered the LWR model with Greenshield's fundamental diagram, and the case study in the conference paper involved synthetic data resembling the traditional loop detector data. In this paper, a framework for using PIDL with CTM is devised, and the incorporation of multiple fundamental diagrams is demonstrated. We introduce two new case studies a) synthetic data resembling CAV data collected by RSUs, and b) the scantily collected probe vehicle data using the NGSIM dataset. The case studies demonstrate
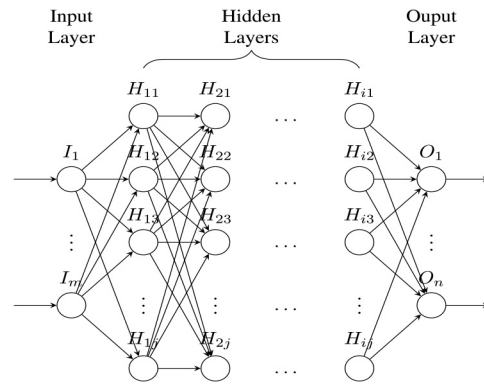


**FIGURE 2.** Architecture of a Deep Learning Neural Network.

the capability of PIDL in traffic state estimation under various scenarios. Hence, both theoretical and experimental contributions are enriched in this paper.

*Outline:* The rest of the paper is organized as follows: Section II provides the background of deep learning neural networks. Section III reviews traffic flow theory and the conservation law as the physical law in TSE. Section IV proposes the integration of physics and deep learning in the estimation of traffic states. Section V presents the first case study using simulated data. Section VI presents the second case study with the Next Generation Simulation (NGSIM) data. Section VII provides a discussion on the usage of physics as a regularization agent in training neural network approaches. Finally, section VIII concludes the paper and suggests future work.

## II. DEEP LEARNING NEURAL NETWORK

The data-driven approach of TSE addresses the tasks of estimation and prediction using only the data collected on the roads. It applies the rapidly emerging machine learning (ML) techniques to recognize the relationship between traffic state variables. The ML algorithm adapts to the particular environment pattern, such as congestion or rush-hour traffic, based on the input data it gets in real-time. Because of its adaptability, the data-driven TSE result is expected to be more reliable when a traffic pattern anomaly is present compared to a model-based approach.

Deep learning (DL) neural network is a subset learning method of ML techniques. The topology of a DL neural network consists of sequential layers of neurons, which are computation units resembling the biological neurons. The three types of layers are *input layer*, where input data are accepted; *output layer*, where output is produced; and *hidden layer*, where information is processed in between. The architecture of a typical deep learning feedforward neural network is drawn in Fig. 2.

A few essential components that warrant contemplation when building a DL neural network are as follows:

*Learning Rate* - It determines the steps in adjusting the value of weights in the neural network. A relatively large

learning rate has the advantage of quicker convergence, producing the prediction results in a shorter period. However, it may omit the better weight configuration and therefore sacrifice the output accuracy.

*Network Size* - The network size is determined by the number of layers $n_l$ and the number of hidden units $n_h$. It reflects the complexity of the neural network, which also has an impact on output accuracy. A complex neural network may be beneficial in yielding accurate results, but it may also be prone to over-fitting [31], and generally takes a long time for convergence.

*Cost Function* - Also known as loss function, it reflects the performance of a trained neural network. The purpose of training a neural network is to adjust its weights to minimize the cost. Various measurements can be used to build cost functions. For instance, (1) gives a cost function using mean square error (MSE), in which $N_o$ is the number of observation points for training. Using vehicle density $\rho$ as an example, $\hat{\rho}(x, t)$ is the estimation of $\rho$ at location $x$ and time $t$.

For $(x, t) \in \mathbb{R} \times \mathbb{R}^+$:

$$
\begin{aligned}
J_{DL} &= MSE_{(\hat{\rho}(x,t), \rho(x,t))} \\
&= \frac{1}{N_o} \sum_{j=1}^{N_o} \left| \hat{\rho}\left(x^{(j)}, t^{(j)}\right) - \rho\left(x^{(j)}, t^{(j)}\right) \right|^2.
\end{aligned} \tag{1}
$$

*Optimization* - Gradient descent is a popular algorithms to perform optimization [32]. It minimizes the cost function $\mathcal{J}(\theta)$ by updating the parameters $\theta \in \mathbb{R}$ in the opposite direction of the gradient of $\mathcal{J}(\theta)$ with respect to the parameters. Batch gradient descent (BGD), mini-batch gradient descent (m-BGD), and Stochastic gradient descent (SGD) are some of the most common methods in the groups of techniques used in search of local minimum.

BGD is formulated as (2). The step it takes to update the parameters is the learning rate $\eta$. It calculates each update using the entire training set; this can be very slow, and it doesn't allow online model updates.

$$
\Delta \theta = -\eta \cdot \nabla_\theta \mathcal{J}(\theta). \tag{2}
$$

SGD circumvents BGD's problem of redundancy by updating the parameters for each training sample. However, the frequent corrections cause high levels of fluctuation in the value of the cost function. m-BGD takes advantage of both algorithms and updates the parameters using a mini-batch of training samples, reducing the variance of samples and the time of convergence.

*Convergence Time* - is the time a neural network takes to converge; we included this measure as estimation of traffic states in real-time is preferable in traffic management [33]. A longer computation time from a complex neural network limits its adaptability for application.

Deep learning for TSE can swiftly modify its weights configuration based on real-time data. However, sensor and detection bias may be introduced in the estimation due to the limited availability of traffic data, hindering the reliability of learning results. Besides, computation capacity is critical to process the extensive incoming traffic data promptly. It compels constructing the computational infrastructure of a higher standard, including data servers and processing centers, to support this data-driven approach.

*Relative Percent $\mathcal{L}_2$ Error* - measures the performance of neural network output. After training, the relative error is evaluated based on the neural network's estimation of the test data. A normalized error measurement using Frobenius norm is shown in (3). $\mathbf{P}$ is the matrix form of vehicle density $\rho(x, t)$, and $\hat{\mathbf{P}}$ is the estimation of $\mathbf{P}$, where $(x, t) \in \mathbb{R} \times \mathbb{R}^+$. Let $N_1$ and $N_2$ be the number of bins after discretizing the density field in space and time, respectively. I.e., $N_1 \cdot N_2$ is the total number of grid points to be estimated. Note that this error formulation is also referred to as root mean square percentage error (RMPSE).

$$
\begin{aligned}
\mathcal{L}_2^{error} &= \frac{\left\| \mathbf{P} - \hat{\mathbf{P}} \right\|_F}{\|\mathbf{P}\|_F} \times 100\% \\
&= \frac{\sqrt{\sum_{j=1}^{N_1 \cdot N_2} \left| \hat{\rho}\left(x^{(j)}, t^{(j)}\right) - \rho\left(x^{(j)}, t^{(j)}\right) \right|^2}}{\sqrt{\sum_{j=1}^{N_1 \cdot N_2} \left| \rho\left(x^{(j)}, t^{(j)}\right) \right|^2}} \times 100\%.
\end{aligned} \tag{3}
$$

*Regularization* - Regularization is a group of methods used to prevent over-fitting when fit a function or a model appropriately on the given training set [34]. With the learned set of parameters $W$, a regularization term can be formulated as (4). $M$ represents the number of parameters in $W$. The associated penalty $\mathcal{E}$ (cost) becomes L1-norm (Lasso regularization) when $q = 1$ and L2-norm (Ridge regularization) when $q = 2$.

$$
\mathcal{E} = \sum_{j=1}^{M} |w_j|^q. \tag{4}
$$

*Automatic Differentiation (AD)* - Also called algorithmic differentiation, AD is a set of techniques for precisely and efficiently evaluating the derivative of numeric functions specified by the computational algorithm. It substitutes the domain of the variables to assimilate the derivative values and replaces the operators per the chain rule to propagate the derivatives [35].

AD addresses the weakness of alternative groups of computation methods: susceptibility of error in manual differentiation [36] and numerical differentiation, due to round-off and truncation errors [37]; and the enigmatic, complex expression resulting from symbolic differentiation [38]. To deploy the standard optimization methods such as LM-BFGS in deep learning, AD produces quantitative derivative evaluations instead of expressions, benefiting the computational accuracy and efficiency [35].

## III. THE PHYSICS OF TRAFFIC FLOW
The traffic flow model and the fundamental diagram are two critical elements of the traffic flow theory.

## A. FLOW MODELS

Traffic flow models use empirical data and the developed hypotheses to model traffic conditions [39]. Let the flow rate $q$ indicate the number of vehicles that pass a set location in a unit of time. Average speed $v$ is the mean value of speed among vehicles traveling on a road segment. Density $\rho$ represents the number of vehicles in a unit road of space. Together, these quantities narrate the temporal and spatial development of traffic conditions.

At a specified location $x$ and a designated time $t$, flow $q(x, t)$ and density $\rho(x, t)$ have the following relationship with the cumulative flow $\mathcal{N}(x, t)$: Cumulative flow $\mathcal{N}(x, t)$ depicts the number of vehicles which have passed location $x$ by the time $t$. Density $\rho(x, t)$ is the partial differential of cumulative count $\mathcal{N}(x, t)$ with respect to $x$. Flow $q(x, t)$ is the partial differential of cumulative count $\mathcal{N}(x, t)$ with respect to $t$. These connections between variables are exhibited in (5).

$$
\begin{cases}
\rho(x, t) = -\dfrac{\partial \mathcal{N}(x, t)}{\partial x} \\[2mm]
q(x, t) = \dfrac{\partial \mathcal{N}(x, t)}{\partial t}
\end{cases}
\tag{5}
$$

There are several traffic flow models discussed in the literature. Continuous-time models include the Lighthill-Whitham-Richards (LWR) model, along with higher-order models such as Payne-Whitham (PW) model [14], [15], Aw-Rascle-Zhang (ARZ) model [16], [17]. Discretized models include cell transmission model (CTM) [12] and switching mode model (SMM) [13]. The first order LWR Model and its discretized version CTM model are the most used traffic flow models for their simplicity and accuracy. We use these two models as the 'physics' of the system and incorporate them into the PIDL framework. These two models are explained next.

## B. LWR MODEL

When the cumulative count $\mathcal{N}(x, t)$ is differentiable in both the time and space domain, Lighthill-Whitham-Richards (LWR) model [40], [41] relates $\mathcal{N}(x, t)$ with flow $q(x, t)$ and density $\rho(x, t)$. Equation (5) leads to the conservation law of traffic flow, given by (6), which is referred to as LWR traffic flow partial differential equation (PDE).

For $(x, t) \in \mathbb{R} \times \mathbb{R}^{+}$:

$$
\frac{\partial q(x, t)}{\partial x} + \frac{\partial \rho(x, t)}{\partial t} = 0.
\tag{6}
$$

### 1) GENERALIZED SOLUTIONS OF LWR

For a conservation law

$$
\rho_t + [q(\rho)]_x = 0
\tag{7}
$$

with the initial condition

$$
\rho(x, 0) = \rho_0(x),
\tag{8}
$$

where $\rho_0 \in L^1_{loc}(\mathcal{R}; \mathcal{R})$, for a given smooth vector field $q : \mathcal{R} \to \mathcal{R}$ the solution in the distributional sense is defined as follows [42]:

Definition 1: A measurable locally integrable function $\rho(x, t)$ is a solution in the distributional sense of the Cauchy problem (7) if for every $\phi \in C_0^\infty(\mathcal{R} \times \mathcal{R}^+) \to \mathcal{R}$

$$
\iint_{\mathcal{R}^+ \times \mathcal{R}} \left[ \rho(x, t)\, \phi_t(x, t) + q(\rho(x, t))\, \phi_x(x, t) \right]\, dx\, dt
$$
$$
+ \int_{\mathcal{R}} \rho_0(x)\, \phi(x, 0)\, dx = 0.
\tag{9}
$$

### 2) WEAK SOLUTIONS

A measurable locally integrable function $\rho(t, x)$ is a weak distributional solution of the Cauchy problem (7) if it is a distributional solution in $(0, T) \times \mathcal{R}$ satisfying (8) and if $\rho$ is a continuous function from $[0, T]$ into $L^1_{loc}$. If we assume $\rho(x, t) = \rho(x^+, t)$, then the continuity condition can be formulated as

$$
\lim_{t \to 0} \int_{\mathcal{R}} |\rho(x, t) - \rho_0(x)|\, dx = 0.
\tag{10}
$$

These conditions give meaning to sets of measure zero for functions in $L^1$. For an $L^1$ function established on the two dimensions $(x, t)$, the domain given by $t = 0$ is a set of measure zero.

Therefore, to implement an initial function in this context we necessitate the $L^1$ continuity of the map $t \to \rho(\cdot, t)$ as exhibited in equation (10). Furthermore, we also necessitate establishing the function's boundary value for a given $x$ value for a fixed time $t$. This is achieved by requiring $\rho(x, t) = \rho(x^+, t) = \lim_{\omega \to x^+} \rho(\omega, t)$. For further details refer to [42].

The traffic density equation should be consistent with the entropy Kružkov solution (see [43]).

Definition 2 (Kružkov Solution): The Kružkov entropy solution is a function $\rho : [0, \infty) \to L^1_{loc}(\mathcal{R})$, such that $\forall k \in \mathcal{R}, \phi > 0 \in C_0^\infty(\mathcal{R} \times \mathcal{R}^+)$ with the compact support of $\phi$ is in $t > 0$, assuming the flow $q$ locally Lipschitz, we have

$$
\iint \left[ |\rho - k|\phi_t + (q(\rho) - q(k))\, \mathrm{sgn}(\rho - k)\phi_x \right] dx\, dt \geq 0.
\tag{11}
$$

and there exists a set $E$ of zero measure on $[0, T]$, such that for $t \in [0, T] - E$, the function $\rho(x, t)$ is defined almost everywhere in $\mathcal{R}$, and for any ball $K_r = \{|x| \leq r\}$

$$
\lim_{t \to 0} \int_{K_r} |\rho(x, t) - \rho_0(x)|\, dx = 0.
\tag{12}
$$

It is essential to point out that Kružkov entropy solutions have been proved equivalent to vanishing viscosity solutions for hyperbolic conservation laws [42], [44].

## C. CTM MODEL

Cell transmission model (CTM) is a discretized model which represents the traffic by dividing the road into consecutive homogeneous sections (cells) [12]. Each cell is created with
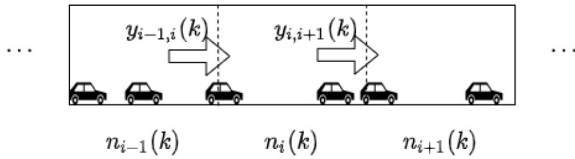
**FIGURE 3.** Cell Transmission Model (CTM) of Traffic Flow.



**FIGURE 4.** Greenshields' Fundamental Diagram.



**FIGURE 5.** Daganzo's Fundamental Diagram.

the equal length $l = v_f \cdot \Delta t$, in which $v_f$ is the free-flow speed. Vehicle flow enters the cell downstream as shown in Fig. 3: $y_{i-1,i}(k)$ represents the flow from upstream cell $i-1$ to downstream cell $i$ at time step $k$, and $y_{i,i+1}(k)$ represents the flow from upstream cell $i$ to downstream cell $i+1$ at time step $k$. $n_{i-1}(k)$, and $n_{i+1}(k)$ conveys the numbers of vehicle in each cell at time step $k$. The resultant flow at the junction of two cells is determined using Godunov approach described in the later sections.

The flow of vehicles between the cells and the number of vehicles present in them comply with (13), in which $n_i(k)$ represents the number of vehicles present in cell $i$ at time step $k$; and $y_{i-1,i}(k)$ represents the vehicle flow from cell $i-1$ to $i$ at time step $k$. For $i \in \mathbb{Z}^+, k \in \mathbb{Z}^+$:

$$n_i(k+1) - n_i(k) = y_{i-1,i}(k) - y_{i,i+1}(k). \quad (13)$$

CTM was initially proposed using a trapezoidal fundamental diagram, in which the flow-density relationship is formulated as (14). The road capacity is $q_m$, and the backward wave speed is $-w$.

$$q = \min\{\rho v_f, q_m, w(\rho_m - \rho)\}. \quad (14)$$

### D. FUNDAMENTAL DIAGRAMS
The fundamental diagram of traffic flow gives the relationship between traffic states - density $\rho$, flow $q$, and speed $v$. It enables modeling the driving behavior from the observed data [45]. Several representations of fundamental diagrams exist; the one proposed by Greenshields [46] is widely used due to its simplicity and the linear relationship between $v$ and $\rho$.

The Greenshields model is shown in Fig. 4.

Greenshields fundamental diagram sets the relationship between traffic state variables as in (15), where $\rho_m$ is the jam density (also known as maximum density), and $v_f$ is the free-flow speed.

$$\begin{cases} q(\rho) = \rho v_f \left(1 - \dfrac{\rho}{\rho_m}\right) \\ v(\rho) = v_f \left(1 - \dfrac{\rho}{\rho_m}\right) \end{cases} \quad (15)$$

Daganzo has offered an alternative model to represent the flow-density relationship by two straight lines, introducing a third parameter—critical capacity $q_c$—at which the maximum flow is reached [47]. Daganzo's fundamental diagram
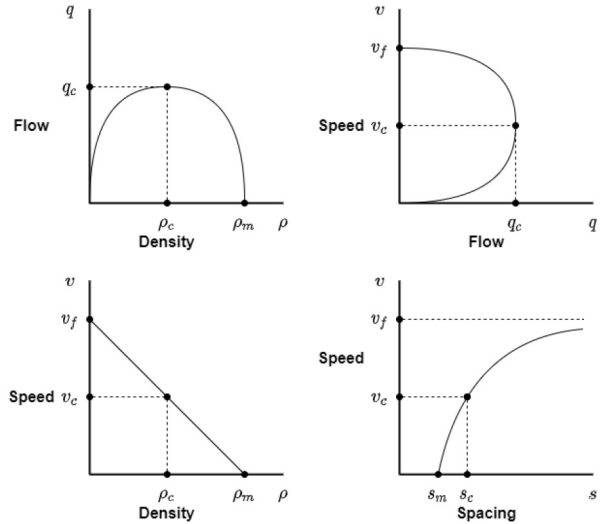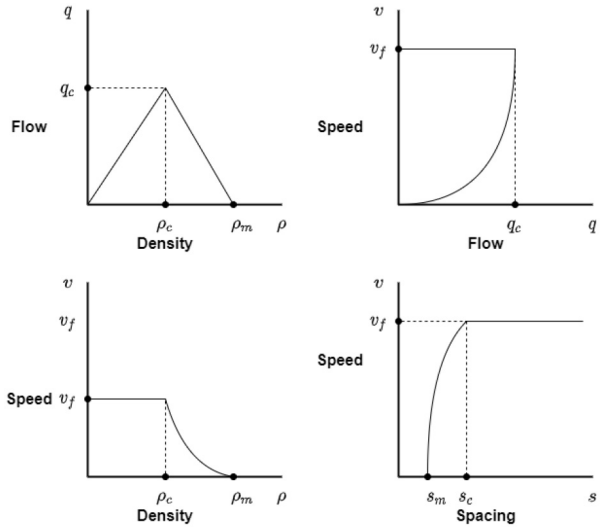
is presented in Fig. 5, and the formulation is shown in (16).

$$q(\rho) = \begin{cases} q_c \dfrac{\rho}{\rho_c} & \text{if } \rho \le \rho_c, \\ q_c \left(1 - \dfrac{\rho - \rho_c}{\rho_m - \rho_c}\right) & \text{if } \rho > \rho_c, \end{cases} \quad (16)$$

Often, a capacity drop is observed when traffic density reaches $\rho_c$. Thus a modification of Daganzo's fundamental diagram—inverse-lambda shaped fundamental diagram—was proposed to reflect this phenomenon [48]–[50]. The modified fundamental diagram is exhibited in Fig. 6, and the relationship between the traffic states is given in (17). The adjusted parameter $q_c$ now is split into two values - $q_{c1}$
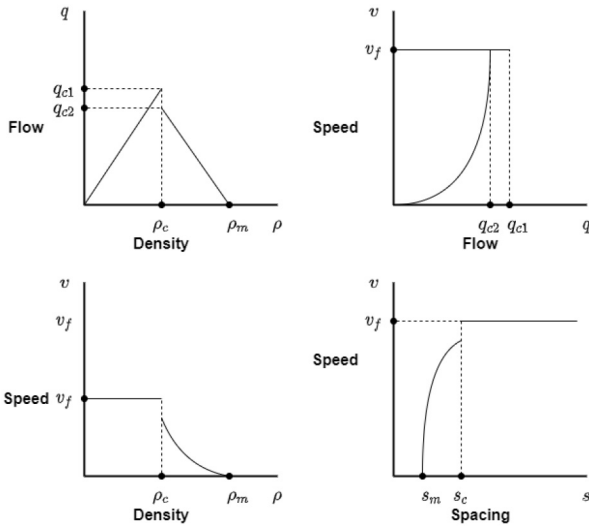
**FIGURE 6.** Inverse-lambda Fundamental Diagram.

before the capacity drop, and $q_{c2}$ after the drop.

$$q(\rho) = \begin{cases} q_{c1} \dfrac{\rho}{\rho_c} & \text{if} \quad \rho \le \rho_c, \\ q_{c2}\left(1 - \dfrac{\rho - \rho_c}{\rho_m - \rho_c}\right) & \text{if} \quad \rho > \rho_c. \end{cases} \quad (17)$$

## IV. PHYSICS INFORMED DEEP LEARNING FOR TRAFFIC STATE ESTIMATION

Physics informed deep learning (PIDL) is a type of DL method where a neural network is trained to solve learning tasks while *respecting the law of physics* [51]. With the inherent physical laws encoded as a priori knowledge, the resulting neural network forms data-efficient approximators to process input information and give reconstruction/prediction results [52]. When the input data is inadequate (scanty) or noisy, the physics in PIDL augments the neural network to use the data effectively. Physics explains the underlying relationship in the data and improves the prediction results.

Therefore, given the unique advantage of PIDL in efficiently utilizing limited input data and the physics (conservation law of traffic flow), we propose physics-informed deep learning for traffic state estimation problems. It combines the strengths of the underlying physical law of the system and the deep learning method in exploiting sparsely observed traffic data for TSE.

### A. PROBLEM FORMULATION

Let $\mathcal{P} = \mathcal{X} \times \mathcal{T}$ be a space-time domain and $\rho(x, t)$ represents the value of the field at $(x, t) \in \mathcal{P}$. On a given road $\mathcal{X}$, $x^j \subset \mathcal{X}$ are the discretized homogeneous road segments and $t^j \subset \mathcal{T}$ are the time intervals.

In $\mathcal{P}$, sparse data of the field $\rho(x, t)$ at $(x_o^j, t_o^j)$ are observed. Collectively, the observed $(x_o^j, t_o^j)$ constitutes a sub-domain $\mathcal{O} \subset \mathcal{P}$. Given that $\forall \ (x, t) \in \mathcal{O}$, $\rho(x, t)$ is known, the reconstruction and prediction problem becomes

finding a mapping function $F(\cdot) : \rho(\mathcal{O}) \rightarrow \rho(\mathcal{P})$, which minimizes the reconstruction cost of $\rho(\mathcal{P})$.

### B. APPROACH OVERVIEW

The PIDL algorithm for TSE is as follows. After splitting the collected traffic state dataset into training and testing datasets, PIDL makes an estimation based on the training dataset. Both estimation cost and physics cost are computed from the estimation result. The neural network gains the knowledge of the governing physical law by incorporating the non-compliance cost of conservation law $J_{PHY}$ into the cost function $\mathcal{J}$. The training iteration is repeated if the sum of estimation cost and physics cost is greater than the designated threshold. Otherwise, the fine-tuned PIDL gives the estimation as output. A maximum of allowed learning iterations - $i_{max}$ is set to prevent the learning process from running eternally in the event of no change in total cost. These steps are graphically presented in Fig. 7. The design of the cost function is one of the primary components of PIDL. Next, we illustrate the design of cost functions using LWR and CTM traffic flow models.

### C. COST FUNCTION USING LWR MODEL

We present the cost function formulation using the hydrodynamic LWR conservation model coupled with Greenshields' and inverse-lambda fundamental diagrams. The conservation law of traffic flow described in (6) establishes the relationship of traffic state variables with respect to location $x$ and time $t$. It needs to be integrated into the learning process of a PIDL neural network. We establish two measures to evaluate the estimation performance. 1) DL-cost, $J_{DL}$, denoting the error in estimation while using just the DL. 2) physics cost, $J_{PHY}$, denoting the disobedience of conservation law in the estimation. The DL-cost utilizes the observed data $\mathcal{O} = \{(x_o^j, t_o^j)|j = 1, 2, \dots, N_o\}$. Whereas the physics cost is computed on the collocation points $\mathcal{C} = \{(x_c^j, t_c^j)|j = 1, 2, \dots, N_c\}$. Note that since the DL estimates the entire grid, there is no restriction on the number of collocation points. Meaning that collocation points (where the physics cost is computed) are not restricted to the observation points, rather they can be any subset of the entire grid points.

*LWR and Greenshields' Model:* The relationship between density $\rho$ and traffic flow $q$ from Greenshields' fundamental diagram (15) transforms the conservation law (6) into (18).

$$v_f\left(1 - \frac{2\rho(x, t)}{\rho_m}\right)\frac{\partial \rho(x, t)}{\partial x} + \frac{\partial \rho(x, t)}{\partial t} = 0 \quad (18)$$

Consequently, we can further formulate the DL-cost $J_{DL}$ and physics cost $J_{PHY}$ as (19):

$$\begin{cases} J_{DL} = \dfrac{1}{N_o} \sum_{j=1}^{N_o} \left| \rho\left(x_o^j, t_o^j\right) - \hat{\rho}\left(x_o^j, t_o^j\right) \right|^2 \\ J_{PHY} = \dfrac{1}{N_c} \sum_{j=1}^{N_c} \left| v_f\left(1 - \dfrac{2\hat{\rho}\left(x_c^j, t_c^j\right)}{\rho_m}\right)\dfrac{\partial \hat{\rho}\left(x_c^j, t_c^j\right)}{\partial x} + \dfrac{\partial \hat{\rho}\left(x_c^j, t_c^j\right)}{\partial t} \right|^2 \end{cases}$$
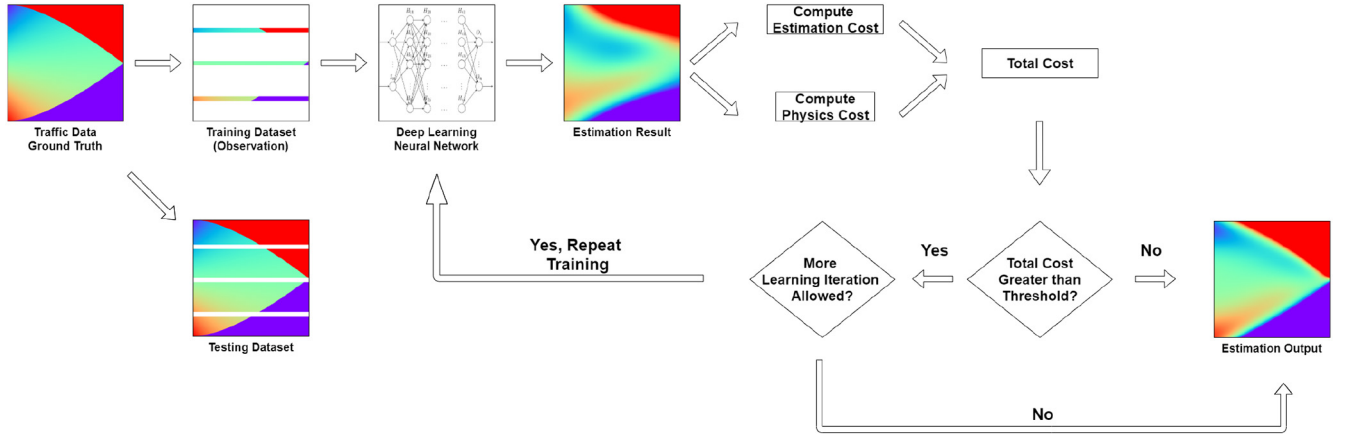
$$(19)$$

**FIGURE 7.** Physics Informed Deep Learning for Traffic State Estimation.

where $\hat{\rho}(x^j, t^j)$ is the estimated density by the DL component of the PIDL approach.

*LWR and Inverse-Lambda Model:* When using the inverse-lambda fundamental diagram, given the relationship between traffic state variables flow $q$ and density $\rho$ in (17), the physics cost $J_{PHY}$ can be formulated as (20). Note that the DL cost ($J_{DL}$) remains the same as shown previously for the Greenshields' model. The collocation points in this case are separated into two subsets $C_1 = \{(x_{c1}^v, t_{c1}^v)|v = 1, 2, \ldots, N_{c1}\}$ where $\hat{\rho}(x_{c1}^v, t_{c1}^v) \leq \rho_c$, and $C_2 = \{(x_{c2}^w, t_{c2}^w)|w = 1, 2, \ldots, N_{c2}\}$ where $\hat{\rho}(x_{c2}^w, t_{c2}^w) > \rho_c$.

$$
\begin{cases}
J_{PHY1} = \dfrac{1}{N_{c1}} \sum_{v=1}^{N_{c1}} \left| \dfrac{\partial \hat{\rho}(x_{c1}^v, t_{c1}^v)}{\partial t} + \dfrac{q_{c1}}{\rho_c} \dfrac{\partial \hat{\rho}(x_{c1}^v, t_{c1}^v)}{\partial x} \right|^2 \\[12pt]
J_{PHY2} = \dfrac{1}{N_{c2}} \sum_{w=1}^{N_{c2}} \left| \dfrac{\partial \hat{\rho}(x_{c2}^w, t_{c2}^w)}{\partial t} - \dfrac{q_{c2}}{\rho_m - \rho_c} \dfrac{\partial \hat{\rho}(x_{c2}^w, t_{c2}^w)}{\partial x} \right|^2 \\[12pt]
J_{PHY} = \dfrac{N_{c1} \cdot J_{PHY1} + N_{c2} \cdot J_{PHY2}}{N_{c1} + N_{c2}}
\end{cases}
$$

$$(20)$$

note that $N_{c1}$ and $N_{c2}$ are the number of collocation points in the free flow region and congested region, respectively; $\hat{\rho}(x_{c1}^v, t_{c1}^v)$ and $\hat{\rho}(x_{c2}^w, t_{c2}^w)$ are the estimated density by the DL component of the PIDL approach.

To incorporate the conservation law of traffic flow in training a PIDL neural network, the cost function of PIDL is comprised of the DL-cost $J_{DL}$ and the physics cost $J_{PHY}$. Hyperparameter $\mu$ is introduced to adjust the weights of $J_{DL}$ and $J_{PHY}$. The cost function $\mathcal{J}$ of PIDL for TSE is given as (21):

$$\mathcal{J} = \mu * J_{DL} + (1 - \mu) * J_{PHY}. \quad (21)$$

### D. COST FUNCTION USING CELL TRANSMISSION MODEL (CTM)

Now we present the cost function formulation using the discrete CTM. Note that it can be coupled with any suitable fundamental diagram. Recall that CTM solves the LWR PDE through a finite difference scheme, also referred to as
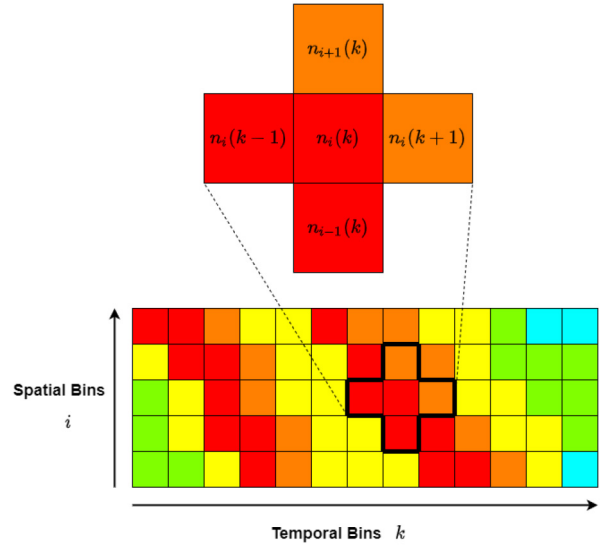


**FIGURE 8.** Discretization of space-time in CTM.

Godunov's numerical method. Consider a spatial-temporal representation of traffic states illustrated in Fig. 8 where the colors denote the variety of traffic state values. Let $N_1$ and $N_2$ be the number of bins after discretizing the density field in space and time, respectively. Thus, $N_1 \cdot N_2$ is the total number of grid points to be estimated.

Making the algorithm conform to the CTM model will lead to the following physics cost:

$$
J_{PHY} = \frac{1}{N_1 \cdot N_2} \sum_{i=1}^{N_1} \sum_{k=1}^{N_2} \left| \left[ \hat{n}_i(k+1) - \hat{n}_i(k) \right] \right.
$$
$$
\left. - \left[ \hat{y}_{i-1,i}(k) - \hat{y}_{i,i+1}(k) \right] \right|^2. \quad (22)
$$

Recall that CTM assumes uniform density $\rho$ in cells at each time step ($n_i(k) = \rho_i(k) \cdot \Delta x$) and uniform flow $q$ between cells during each time interval ($y_{i-1,i}(k) = q_{i-1,i}(k) \cdot \Delta t$). Therefore, the DL-cost and the physics cost

with CTM become as follows:

$$\begin{cases} J_{DL} = \dfrac{1}{N_o} \sum_{j=1}^{N_o} \left| \rho\left(x_o^j, t_o^j\right) - \hat{\rho}\left(x_o^j, t_o^j\right) \right|^2 \\ J_{PHY} = \dfrac{1}{N_1 \cdot N_2} \sum_{i=1}^{N_1} \sum_{k=1}^{N_2} \left| \left[ \hat{\rho}_i(k+1) - \hat{\rho}_i(k) \right] \cdot \Delta x \right. \\ \qquad\qquad \left. - \left[ \hat{q}_{i-1,i}(k) - \hat{q}_{i,i+1}(k) \right] \cdot \Delta t \right|^2. \end{cases}$$
(23)

Similar to the previous discussion on the LWR model, the cost function of PIDL is comprised of the DL-cost $J_{DL}$ and the physics cost $J_{PHY}$ given in (23). Note that $J_{DL}$ is computed in a similar fashion using $N_o$ observations. Whereas, the formulation of $J_{PHY}$ differs from the LWR case. Also, unlike the case of LWR, here we use the entire grid ($N_1 \cdot N_2$) as collocation points. This makes the representation easier, however, a subset of $N_1 \cdot N_2$ can also be used. Hyperparameter $\mu$ can adjust the weights of $J_{DL}$ and $J_{PHY}$ as shown in (21).

The computation of flow ($q_{i-1,i}$) between the adjacent cells $i - 1$ and $i$ is described next. The density conditions of both cells determine the flow rate at the boundary of two adjacent cells. It can be computed using Godunov's numerical scheme [11], [53]. The Godunov method discretizes the first-order traffic flow models such as the LWR model by solving the Riemann problem with the initial condition of upstream density $\rho_{i-1}$ and downstream density $\rho_i$ [44].

Either a shockwave or a rarefaction wave will originate from the junction of the two densities. A shockwave develops when $q'(\rho_{i-1}) > q'(\rho_i)$, and a rarefaction develops when $q'(\rho_{i-1}) < q'(\rho_i)$. The speed of the shockwave is given by:

$$s = \frac{dx_s(t)}{dt} = \frac{\left[ q(\rho_{i-1}) - q(\rho_i) \right]}{\rho_{i-1} - \rho_i}$$
(24)

where $x_s(t)$ is the position of the shockwave as a function of time. If the shock speed is positive, then the inflow at the junction between the two traffic densities will be a function of upstream traffic density. In contrast, if the shockwave speed is negative, then the inflow at the junction between the two traffic densities will be a function of downstream traffic density.

Let $Q(\cdot, \cdot)$ be a function denoting the flow at the boundary of two cells which can be determined as follows:

$$Q(\rho_{i-1}, \rho_i) = q\left( \rho^*(\rho_{i-1}, \rho_i) \right)$$
(25)

where $\rho^*$ denotes the flow-dictating density. $\rho^*$ is determined by the following relationship emanating from the Godunov scheme:

$$\rho^* = \begin{cases} \rho_{i-1}, & \text{if} \quad q'(\rho_{i-1}), q'(\rho_i) \geq 0 \\ \rho_i, & \text{if} \quad q'(\rho_{i-1}), q'(\rho_i) \leq 0 \\ \rho_{i-1}, & \text{if} \quad q'(\rho_{i-1}) \geq 0 \geq q'(\rho_i) \\ & \quad \text{and} \quad q(\rho_{i-1}) > q(\rho_i) \\ \rho_i, & \text{if} \quad q'(\rho_{i-1}) \geq 0 \geq q'(\rho_i) \\ & \quad \text{and} \quad q(\rho_{i-1}) < q(\rho_i) \\ \rho_c, & \text{if} \quad q'(\rho_{i-1}) < 0 < q'(\rho_i) \end{cases}$$
(26)

here $\rho_c$ is the critical density.

Hence depending on the traffic densities on the left and right side of the junction, flow at the junction can have three possible values, i.e., $Q(\rho_{i-1}, \rho_i)$ can have three distinct values, $q(\rho_{i-1})$, $q(\rho_i)$, or $q(\rho_c)$. Note that $Q(\rho_{i-1}, \rho_i) = q_{i-1,i}$. Once the flow-dictating density $\rho^*$ is identified, the corresponding flow $q(\rho^*)$ can obtained using any suitable fundamental diagram.

## V. CASE STUDY-I
Case study-I is designed to resemble the application scenario where the trajectory information of connected and autonomous vehicles (CAVs) as captured by roadside units (RSUs) is available for TSE.

### A. DATA DESCRIPTION
Synthetic dataset is constructed mimicking vehicular traffic using the Lax-Hopf method as described in [54]. The testbed consists of a 5000-meter road segment for 300 seconds ($x, \ t \in [0, 5000] \times [0, 300]$). The spatial resolution of the dataset is 5 meters and the temporal resolution is 1 second ($\Delta x = 5, \Delta t = 1$). In this case study, velocity-field $v(x, t)$ is the learning objective of the neural network. The experimental synthetic dataset is shown in Fig. 9. The vehicle trajectory data is produced under the following assumptions and control measures:

1) *Vehicle Speed-Density Relationship:* Greenshields' fundamental diagram formulated is Eq. (15) applies in the relationship between vehicle speed and density. The free flow speed $v_f$ is 25 meters per second (90 kph or 56 mph). The maximum density $\rho_m$ is 0.15 vehicles per meter.
2) *Initial Vehicle Density:* At $t = 0$, density $\rho$ is 0.14 vehicle per meter (veh/m) at $x \in [0, 1500]$, 0.04 veh/m at $x \in [1500, 3500]$, 0.08 veh/m at $x \in [3500, 4000]$, and 0.1 veh/m at $x \in [4000, 5000]$.
3) *Upstream Flow and Downstream Flow:* At $x = 0$, the upstream flow $q_{in}$ is 0.3 vehicle per second (veh/s) at $t \in [0, 60]$, 0.4 veh/s at $t \in [60, 180]$, and
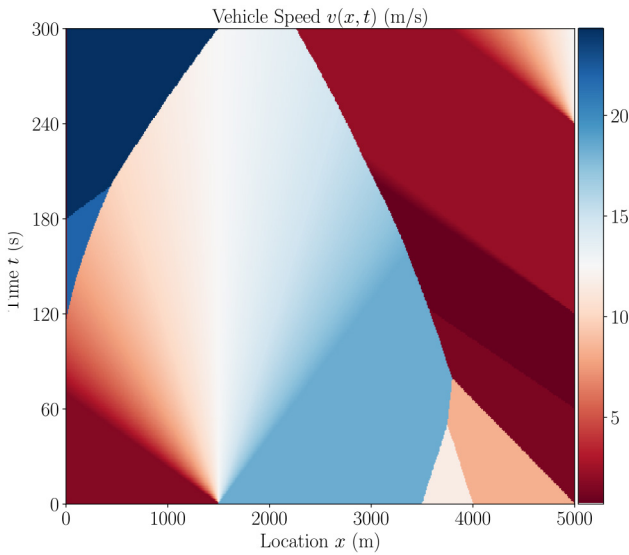
**FIGURE 9.** Experiment Dataset.



**FIGURE 10.** PIDL & DL Estimation with 1% CAV Fleet.

0.1 veh/s at $t \in [180, 300]$. At $x = 5000$, the downstream flow $q_{out}$ is 0.2 vehicle per second (veh/s) at $t \in [0, 60]$, 0.1 veh/s at $t \in [60, 120]$, and 0.3 veh/s at $t \in [120, 240]$ and 0 (to simulate a road closure or traffic accident) at $t \in [240, 300]$.
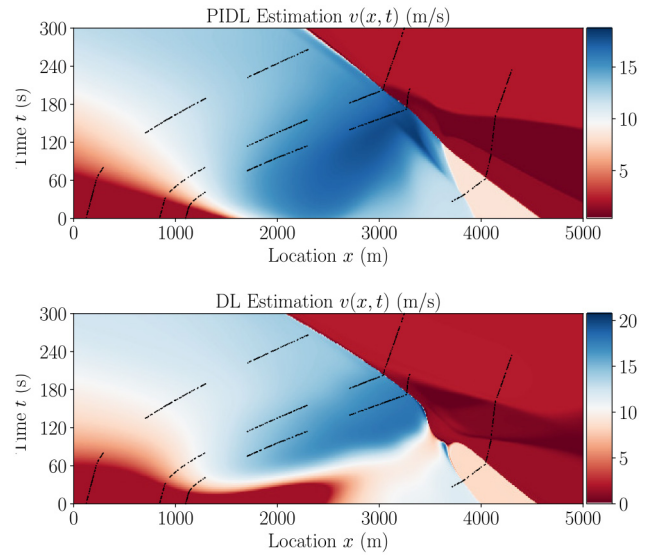
Recall that the case study is designed to utilize the CAV data as collected by RSUs, with the objective to estimate velocity field. It assumes that the RSUs are deployed every 1000 meter on the road segment; therefore, there are 6 RSUs installed on the 5000-meter road (the first one is installed at initial location $x = 0$). Based on [55], the communication range of RSU is assumed to be 300 meters (DSRC technology). That means, vehicle information broadcast by CAVs at $x \in [0, 300]$ can be captured by the first RSU and the second RSU can log CAV data transmitted at $x \in [700, 1300]$. Data broadcasted at $x \in [300, 700]$ however is cutoff to the system. Data loss due to the limitation of the communication range of RSU is also considered. More details on the creation of the synthetic data can be found in [30].

### B. IMPLEMENTATION DETAILS
The PIDL neural network for the experiment is built with a 10-hidden-layer architecture, with 40 neurons on each hidden layer. The optimization algorithm is a limited-memory Broyden-Fletcher-Goldfarb-Shanno (LM-BFGS) algorithm. The maximum learning iteration is 5000. For comparison with PIDL on performance, a deep learning (DL) neural network with the same architecture, however, unaware of the conservation law in traffic flow theory, is also trained in this case study. The experiment is conducted on an `Intel Core i7-8700` CPU @ 3.20GHz.

### C. RESULTS AND DISCUSSION
We perform the analysis with various penetration rates of CAVs in the traffic stream. We use computation time and the percent relative $\mathcal{L}_2$ error metric (defined in (3)) to evaluate the performance. Each neural network's performance is evaluated 3 times using 3 training datasets obtained with different sampling seeds. We also assume that there is a 10 percent data loss; hence 90 percent of the transmitted data within the communication range of RSUs are recorded.

*1% Penetration Rate:* First, we investigate the PIDL approach's performance with a vehicle fleet consisting of 1 percent CAVs and 99 percent conventional vehicles. Under this scenario, only 4 vehicles in the experiment can broadcast information through the vehicle to infrastructure (V2I) communication to RSUs. The estimation results of PIDL and DL (for comparison) are presented in Fig. 10. Vehicle velocity data logged by RSUs are also marked.

*Interpretation:* We notice that with the aid of the physical law of traffic flow, PIDL outperforms DL with higher estimation accuracy and achieves shorter computation time, which means greater feasibility of time-sensitive applications. The physics-informed approach accommodates the reality of (training) data sparsity by leveraging the collocation points. As discussed before, collocation points are coordinate pairs of location and time $(x, t)$ where the physics cost can be computed to quantify the disobedience of current states in terms of the governing conservation law. The physical equations provide tangible insights into the underlying relationship between traffic state variables such as flow and velocity. And the physics cost assessed by PIDL serves as a torchlight guiding the optimization process of parameters in the neural network.

*10% Penetration Rate:* Next, we discuss the performance of the PIDL approach considering a 10 percent CAV fleet. The estimation result is shown in Fig. 11. In both penetration level scenarios, the estimation error and computation time reported are the mean averages of 3 experiments.

*Interpretation:* With the higher availability of vehicle data in this scenario, the accuracy performance of DL is slightly
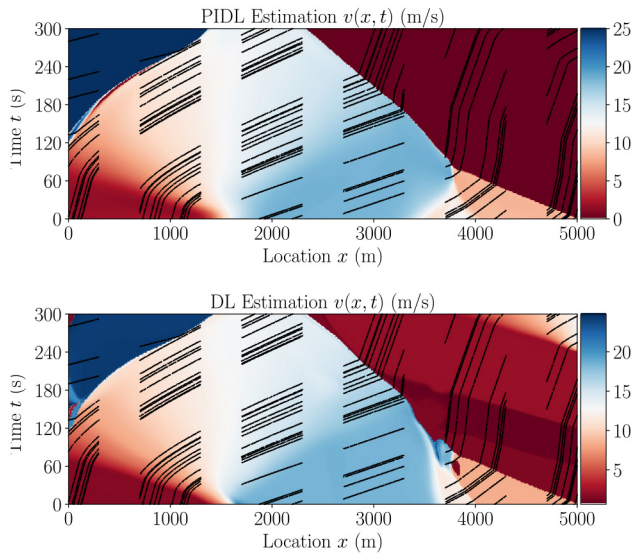
**FIGURE 11.** PIDL & DL Estimation with 10% CAV Fleet.

**TABLE 1.** Sensitivity analysis for various penetration rates.

| CAV Penetration Rate | Computation Time | | Relative $\mathcal{L}_2$ Error (%) | |
|---|---|---|---|---|
| | PIDL | DL | PIDL | DL |
| 1% | **33.7s** | 75.0s | **31.7** | 42.9 |
| 10% | **238.1s** | 473.6s | 16.7 | **13.1** |
| 25% | **379.2s** | 643.8s | **7.2** | 10.8 |
| 50% | **148.6s** | 250.3s | **5.6** | 9.4 |
| 75% | **96.8s** | 124.7s | **6.2** | 8.7 |
| 100% | **21.8s** | 45.1s | **3.4** | 5.6 |

**TABLE 2.** Sensitivity analysis for various noise levels.

| Noise Level | Relative $\mathcal{L}_2$ Error (%) | |
|---|---|---|
| | PIDL | DL |
| 5% | **18.3** | 19.2 |
| 10% | **19.6** | 21.3 |
| 15% | **22.9** | 30.8 |

to examine the performance of PIDL and DL. Even with the best available sensing technology, the consideration of imprecision in the observed traffic state is imperative. Given the synthetic dataset, we fuse the training data with 4 levels of Gaussian noise and compare the performance under the 10% CAV penetration rate scenario. The results are shown in Table 2.

The benefit of physics in training is more evident with added data noise, as the results show PIDL outperforms DL under noisy data scenarios, and the difference is more pronounced as the noise level grows.

*Summary of Results for Case Study-I :*

- The computation time of PIDL is better for all penetration rates.
- For 1% penetration rate, the relative $\mathcal{L}_2$ error for PIDL was 31.7% as compared to 42.9% for DL.
- With a 15% noise added to the sensor data, the relative $\mathcal{L}_2$ error for PIDL was at 22.9% compared to 30.8% for DL.

## VI. CASE STUDY-II

Recall that the second case study is designed to resemble scant observations from probe vehicles using the trajectory information from Next Generation Simulation (NGSIM) data [56]. It examines the performance of the physics-informed deep learning approach in recreating the velocity field. We choose the vehicle trajectory data collected on the interstate 80 freeway (I-80) in Emeryville, California.

### A. DATA DESCRIPTION

The road segment with recorded vehicle trajectory is about 1600 feet long [57], and the vehicle velocity and positional information is extracted from video recordings [58]. The 15-minute vehicle velocity-field obtained from 4:00pm - 4:15pm on April 13$^{th}$, 2005 on I-80 freeway is shown in Fig. 12. Shock waves can be observed in the figure, indicating congestion propagating backward on the freeway.

The velocity field is constructed from vehicle trajectory data using a binning method with spatial resolution $\Delta x$ of 20 feet and the temporal resolution $\Delta t$ of 5 seconds. The average speed of vehicles in each bin is calculated. The resulting velocity-field consists of 180 temporal bins and 80 spatial bins.
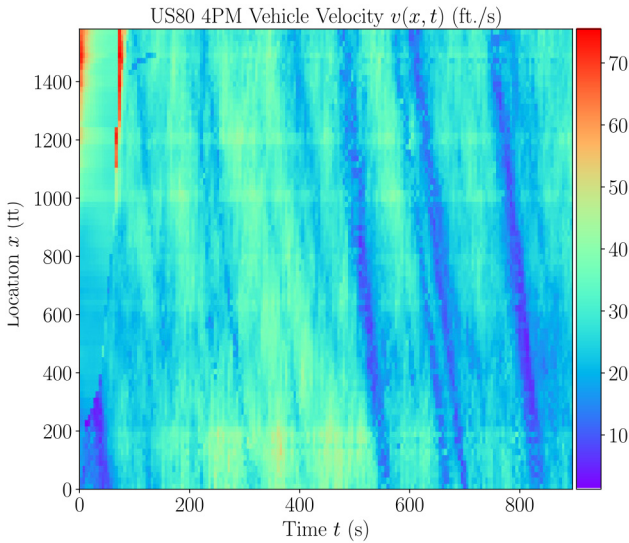
better, suggesting the richness in input data compensates for the absence of physical law awareness. However, the accuracy achieved by DL comes at the expense of computation time. In contrast, PIDL achieves similar estimation accuracy in a much shorter time. The experiment once again demonstrates the benefit of incorporating physical law in training neural networks. We observe that while accomplishing comparable estimation accuracy in some cases, the PIDL method always has the advantage of quick convergence and proves to be a desirable approach for real-time applications.

*25%, 50%, 75%, and 100% Penetration Rate:* Similarly, we analyze the penetration rates of 25%, 50%, 75%, and 100%. Table 1 provides the results for various penetration levels. **Bold** font indicates better performance.

*Interpretation:* With the aid of physics, PIDL consistently surpasses the estimation accuracy metric of DL. We also observe that with the increasing availability of training data as the CAV fleet expands, the time to convergence of PIDL and DL both decreases (when the CAV penetration rate is above 25%). This suggests that with the abundant training data, the estimation tasks are becoming increasingly undemanding, and both neural networks (PIDL & DL) are able to produce the results in shorter periods of time.

*Noise Sensitivity Analysis:* Lastly, we conduct the sensitivity analysis with regard to noise level in the training data

**FIGURE 12.** NGSIM Vehicle Velocity-Field, I-80 Freeway, 4:00pm - 4:15pm.
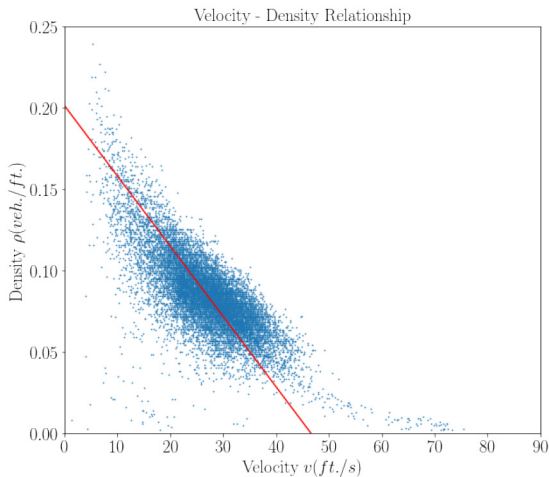


**FIGURE 13.** Parameter Estimation of Critical Traffic States in NGSIM I-80 Freeway, 4:00pm - 4:15pm Dataset.

## B. IMPLEMENTATION DETAILS

The performance of PIDL in regenerating the velocity field is investigated with the acquaintance of a few samples from the NGSIM dataset. The Greenshields' fundamental diagram is deployed to represent the relationship between traffic state variables. The LWR conservation law is still used as the governing physical equation.

The recorded NGSIM data shows vehicles experiencing various levels of congestion [59]. Recall that in the case study-I, the velocity field was built using known values of parameters such as free-flow speed $v_f$ and jam density $\rho_m$. Whereas, in this experiment, traffic parameters are unknown and need to be estimated.

The density-velocity relationship is illustrated in Fig. 13. The estimated values are summarized in Table 3. It is worth pointing out that the vehicle density $\rho$ is the summation of vehicles on the 5 lanes of I-80 freeway in Emeryville, California.

**TABLE 3.** Estimated parameters for Greenshields' fundamental diagram.

| | Free-flow Speed | Jam Density |
|---|---|---|
| **Estimated Parameter Value** | $v_f = 46.64 ft/s$ | $\rho_m = 0.20 veh/ft$ |

Training samples from the velocity field are randomly selected (to mimic scant probe vehicle observations), providing the neural network observations at various spatial-temporal locations.

## C. RESULTS AND DISCUSSION

The reconstructed velocity-field using 1440 (10%) and 2000 (14%) samples are presented in Fig. 14 and Fig. 15. The accuracy of the estimation result is evaluated by using the percent relative $\mathcal{L}_2$ error defined in (3).

We observe from Fig. 14 and Fig. 15 that in both scenarios, PIDL captured the characteristics of the NGSIM data and reconstructed the shockwaves from limited data samples. In contrast, no meaningful traffic insights can be extracted from the velocity field restored by DL. DL neural networks did converge quicker at the expense of reconstruction accuracy. PIDL neural networks underwent noticeably more iterations updating the weight matrices and bias vectors before convergence and acquiring a lower cost value. It highlights the limited training iterations of DL as compared to PIDL. It may be due to the DL algorithm converging to a local minimum.

We also assume a scenario in which the computation capacity is limited, and there is a constraint on the number of training iterations. The performance of PIDL and DL are examined after both neural networks are only allowed 5000 iterations for training. In this case, PIDL still outperforms DL in terms of securing a lower value of cost. The cost and training iterations at convergence and the cost at 5000-iteration limit of PIDL and DL are detailed in Table 4. Better performances are highlighted in **bold**.

Although both neural networks are built upon the same architecture and are given the same training samples, the difference in cost functions provides the PIDL with a unique advantage in efficiently utilizing limited observation and producing estimation. The distinction of the PIDL cost function should be considered when comparing the performance between PIDL and DL based on the cost at convergence.

*Summary of Results for Case Study-II:*

- With 10% data, the relative $\mathcal{L}_2$ error for PIDL was 6.8% compared to 26.7% for DL.
- The experiment results demonstrate that PIDL achieved superior performance in TSE with limited amount of training data, comparing to DL.

*Note:* The github repository containing the data and code can be found at: github.com/Urbanity-Lab/PIDL

## VII. DISCUSSION: PHYSICS AS A REGULARIZATION AGENT

In this section, we reflect back on the proposed approach and case studies, and discuss the applicability of physics as
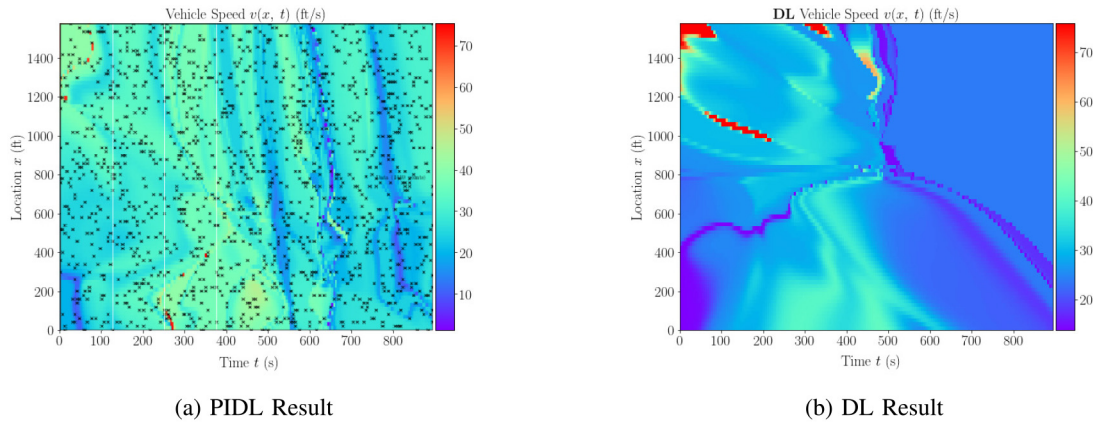
(a) PIDL Result



(b) DL Result

**FIGURE 14.** Reconstructed Velocity-Field based on 1440 (10%) Samples from NGSIM.
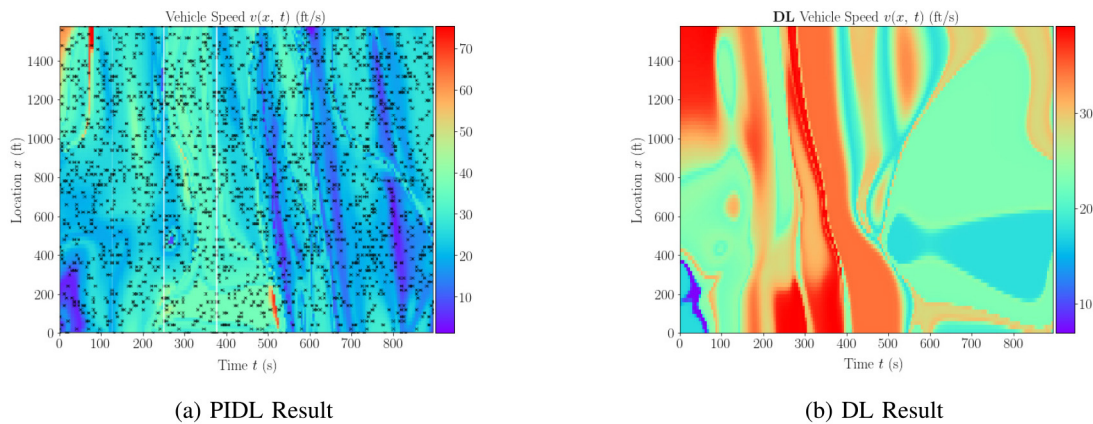


(a) PIDL Result



(b) DL Result

**FIGURE 15.** Reconstructed Velocity-Field based on 2000 (14%) Samples from NGSIM.

**TABLE 4.** PIDL & DL performance comparison.

| Training Samples | Relative $\mathcal{L}_2$ Error (%) at Convergence | | Training Iterations at Convergence | | Relative $\mathcal{L}_2$ Error (%) at 5000-Iteration | |
|---|---|---|---|---|---|---|
| | PIDL | DL | PIDL | DL | PIDL | DL |
| 1440 (10%) | **6.8** | 26.7 | 13014 | 3712 | **8.2** | 26.7 |
| 2000 (14%) | **9.4** | 17.6 | 14693 | 4296 | **10.3** | 17.6 |

a regularization agent in the framework of physics-informed deep learning. Recall the cost function of PIDL in (21); the physics cost can be viewed as a regularization agent of the learning process [60].

Given the limited observation of traffic, a regular neural network has meager input in the training process to identify meaningful parameter values (weights and biases, for instance) needed for traffic state estimation. In order to produce a realistic assessment, procedures need to be considered to prevent both the under-fitting and over-fitting problems for accuracy and robustness. Under this background, laws from the traffic flow theory provide valid guidelines in fitting the model specification to acquire knowledge of the traffic in unobserved areas. It can prevent over/under-fitting training samples by penalizing learning where reconstruction doesn't satisfy the physical law.

*Under-fitting* commonly occurs when the input data is complex, and the structure of a learning model is naive. As pointed out earlier, given the complexity of deep learning models and the limited availability of the training data, under-fitting is not a major concern in our case. Preventing the *over-fitting* problem to ensure the acceptable model performance is the prominent task here. Over-fitting happens when a model brings impaired generalization from observed data into the unseen field [61]. It excessively relies on the training input and loses the ability to adapt to the unseen test data. Regularization counters the issue of over-fitting by reducing the complexity of the model, limiting the weights assigned to features deemed less influential in producing the desired output [62]. It introduces a penalty term to the cost function to restrict the model from learning more features or assigning heavier weights to trivial features during training.

Common practices to avoid over-fitting include "early-stopping", which deals with the phenomenon where testing accuracy ceases to improve after a certain amount of training [63]; "network-reduction" [64], which reduces the size of the learning network to limit model complexity, ultimately to quash the noise or irrelevant information in the training data. Data expansion [65] is another strategy that falls into this category to combat over-fitting by creating more training inputs through either acquisition of new data or re-sampling existing observation points.

However, all the above-mentioned methods have respective shortcomings. In order to implement "early-stopping", the hyper-parameter of the training iteration limit (the point at which training must be stopped), needs to be determined through empirical evidence. Note that a premature stopping induces the "under-fitting" problem. Similarly, "network reduction" necessitates an informed decision on reducing the model complexity while preserving the capacity of learning the underlying relationship presented in the training data. When new data is not easily available, which is often the case with TSE, bias associated with the re-sampling strategy may be introduced in the data expansion process.

By incorporating the physics cost $J_{PHY}$ into the cost function in the "physics-informed" framework, physical laws from the traffic flow theory act as a regularization agent in the training process and let the binding rules of traffic state with respect to space and time play a role in guiding the optimization. It penalizes the parameters and configuration of the neural network that does not comply with the system of laws imposed. This brings improvement in estimation accuracy and convergence time, as are demonstrated in the case studies, owing to two unique advantages.

The *first* advantage of the PIDL model in preventing over-fitting is the information gained supplied by the physics. The partial derivatives of traffic state with respect to time and space in the conservation law reflect the relationship between traffic state in adjacent locations, and the incremental changes as the state evolve. This information on how traffic states transform presents a powerful tool in utilizing the sparse training input by constructing an educated estimation of traffic states at neighboring locations or succeeding timestamps.

The *second* benefit of the incorporation of physics cost $J_{PHY}$, by design, is the introduction of collocation points in the training process. Collocation points are coordinate pairs of location and timestamp $(x, t)$. Albeit the size of training input is small, a much greater amount of collocation points can be selected, and $J_{PHY}$ at collocation points are assessed to verify the compliance with governing laws of physics. In other words, even if the ground truth of traffic state for training is in short supply, the "physics-informed" neural network can calculate the physics cost at any given location $x$ and time $t$ and minimize it. The aforementioned advantages of PIDL are consequential in precise and prompt TSE.
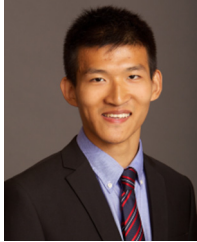
## VIII. CONCLUSION

This paper presented a physics-informed deep learning (PIDL) methodology for traffic state estimation (TSE). Combining the strength of underlying physical laws of traffic flow and deep learning techniques, we demonstrated the capability of PIDL in utilizing scantily available traffic data for accurate and real-time TSE. The approach was presented using LWR and CTM models combined with the Greenshields', Daganzo's, and Inverse-lambda fundamental diagrams. Two case studies were performed to validate the proposed approach. The first case study utilized synthetic data resembling CAV trajectory data as captured by RSUs. The second case study utilized NGSIM data - repurposed to resemble a scantily collected probe vehicle data. Results showed that PIDL is effective in TSE and outperforms the DL method, especially with sparse and unreliable (due to noise and communication loss) measurements. Future work should consider a simultaneous estimation of model parameters and state reconstruction.

## REFERENCES

[1] M. Treiber, A. Kesting, and R. E. Wilson, "Reconstructing the traffic state by fusion of heterogeneous data," *Comput.-Aided Civil Infrastructure Eng.*, vol. 26, no. 6, pp. 408–419, 2011.

[2] N. Bekiaris-Liberis, C. Roncoli, and M. Papageorgiou, "Highway traffic state estimation with mixed connected and conventional vehicles," *IEEE Trans. Intell. Transp. Syst.*, vol. 17, no. 12, pp. 3484–3497, Dec. 2016.

[3] S. Agarwal, P. Kachroo, and S. Contreras, "A dynamic network modeling-based approach for traffic observability problem," *IEEE Trans. Intell. Transp. Syst.*, vol. 17, no. 4, pp. 1168–1178, Apr. 2016.

[4] S. Agarwal and P. Kachroo, "Controllability and observability analysis for intelligent transportation systems," *Transp. Develop. Econ.*, vol. 5, no. 1, p. 2, 2019.

[5] S. Contreras, P. Kachroo, and S. Agarwal, "Observability and sensor placement problem on highway segments: A traffic dynamics-based approach," *IEEE Trans. Intell. Transp. Syst.*, vol. 17, no. 3, pp. 848–858, Mar. 2016.

[6] S. Contreras, S. Agarwal, and P. Kachroo, "Quality of traffic observability on highways with lagrangian sensors," *IEEE Trans. Autom. Sci. Eng.*, vol. 15, no. 2, pp. 761–771, Apr. 2018.

[7] J. C. Herrera and A. M. Bayen, "Incorporation of Lagrangian measurements in freeway traffic state estimation," *Transp. Res. B Methodol.*, vol. 44, no. 4, pp. 460–481, 2010.

[8] S. Agarwal, E. E. Regentova, P. Kachroo, and H. Verma, "Multidimensional compression of ITS data using wavelet-based compression techniques," *IEEE Trans. Intell. Transp. Syst.*, vol. 18, no. 7, pp. 1907–1917, Jul. 2017.

[9] T. Seo, A. M. Bayen, T. Kusakabe, and Y. Asakura, "Traffic state estimation on highway: A comprehensive survey," *Annu. Rev. Control*, vol. 43, no. 43, pp. 128–151, 2017.

[10] E. F. Grumert and A. Tapani, "Traffic state estimation using connected vehicles and stationary detectors," *J. Adv. Transp.*, vol. 2018, Jan. 2018, Art. no. 4106086.

[11] S. Agarwal, P. Kachroo, S. Contreras, and S. Sastry, "Feedback-coordinated ramp control of consecutive on-ramps using distributed modeling and Godunov-based satisfiable allocation," *IEEE Trans. Intell. Transp. Syst.*, vol. 16, no. 5, pp. 2384–2392, Oct. 2015.

[12] C. F. Daganzo, "The cell transmission model: A dynamic representation of highway traffic consistent with the hydrodynamic theory," *Transp. Res. B Methodol.*, vol. 28, no. 4, pp. 269–287, 1994.

[13] L. Muñoz, X. Sun, R. Horowitz, and L. Alvarez, "Piecewise-linearized cell transmission model and parameter calibration methodology," *Transp. Res. Rec.*, vol. 1965, no. 1, pp. 183–191, 2006.

[14] H. J. Payne, *Model of Freeway Traffic and Control*, Math. Model Public Syst., Simulat. Councils, Inc., La Jolla, CA, USA, 1971, pp. 51–61.

[15] G. Whitham, *Linear and Nonlinear Waves*, New York, NY, USA: Wiley, 1974.

[16] A. Aw and M. Rascle, "Resurrection of 'second order' models of traffic flow," *SIAM J. Appl. Math.*, vol. 60, no. 3, pp. 916–938, 2000.

[17] H. M. Zhang, "A non-equilibrium traffic model devoid of gas-like behavior," *Transp. Res. B Methodol.*, vol. 36, no. 3, pp. 275–290, 2002.

[18] J. Thai and A. M. Bayen, "State estimation for polyhedral hybrid systems and applications to the Godunov scheme for highway traffic estimation," *IEEE Trans. Autom. Control*, vol. 60, no. 2, pp. 311–326, Feb. 2015.

[19] T. Schreiter, C. Van Hinsbergen, F. Zuurbier, J. Van Lint, and S. Hoogendoorn, "Data-model synchronization in extended Kalman filters for accurate online traffic state estimation," in *Proc. TFTC Summer Meeting*, 2010, pp. 1–9.

[20] L. Mihaylova, R. Boel, and A. Hegiy, "An unscented Kalman filter for freeway traffic estimation," in *Proc. IFAC*, 2006, pp. 1–6.

[21] Y. Yuan, F. Scholten, and H. van Lint, "Efficient traffic state estimation and prediction based on the ensemble Kalman filter with a fast implementation and localized deterministic scheme," in *Proc. IEEE 18th Int. Conf. Intell. Transp. Syst.*, 2015, pp. 477–482.

[22] L. Li, Y. Li, and Z. Li, "Efficient missing data imputing for traffic flow by considering temporal and spatial dependence," *Transp. Res. C Emerg. Technol.*, vol. 34, pp. 108–120, Sep. 2013.

[23] S. Tak, S. Woo, and H. Yeo, "Data-driven imputation method for traffic data in sectional units of road links," *IEEE Trans. Intell. Transp. Syst.*, vol. 17, no. 6, pp. 1762–1771, Jun. 2016.

[24] N. G. Polson and V. O. Sokolov, "Deep learning for short-term traffic flow prediction," *Transp. Res. C Emerg. Technol.*, vol. 79, pp. 1–17, Jun. 2017.

[25] A. Azzouni and G. Pujolle, "A long short-term memory recurrent neural network framework for network traffic matrix prediction," 2017, *arXiv:1705.05690*.

[26] J. Guo, Y. Liu, Q. Yang, Y. Wang, and S. Fang, "GPS-based city-wide traffic congestion forecasting using CNN-RNN and C3D hybrid model," *Transportmetrica A Transp. Sci.*, vol. 17, no. 2, pp. 190–211, 2021.

[27] Z. Zhao, W. Chen, X. Wu, P. C. Chen, and J. Liu, "LSTM network: A deep learning approach for short-term traffic forecast," *IET Intell. Transport Syst.*, vol. 11, no. 2, pp. 68–75, 2017.

[28] W. Xiangxue, X. Lunhui, and C. Kaixun, "Data-driven short-term forecasting for urban road network traffic based on data processing and LSTM-RNN," *Arab. J. Sci. Eng.*, vol. 44, no. 4, pp. 3043–3060, 2019.

[29] R. Rahman and S. Hasan, "Short-term traffic speed prediction for freeways during hurricane evacuation: A deep learning approach," in *Proc. IEEE 21st Int. Conf. Intell. Transp. Syst. (ITSC)*, 2018, pp. 1291–1296.

[30] J. Huang and S. Agarwal, "Physics informed deep learning for traffic state estimation," in *Proc. IEEE 23rd Int. Conf. Intell. Transp. Syst. (ITSC)*, 2020, pp. 540–547.

[31] C. Dumitru and V. Maria, *Advantages and Disadvantages of Using Neural Networks for Predictions*, Ann. Ser. Econ. Sci., Ovidius Univ., Constanţa, Romania, 2013.

[32] S. Ruder, "An overview of gradient descent optimization algorithms," 2016, *arXiv:1609.04747*.

[33] Y. Wang and M. Papageorgiou, "Real-time freeway traffic state estimation based on extended Kalman filter: A general approach," *Transp. Res. B Methodol.*, vol. 39, no. 2, pp. 141–167, 2005.

[34] C. M. Bishop and N. M. Nasrabadi, *Pattern Recognition and Machine Learning*. New York, NY, USA: Springer, 2006.

[35] A. G. Baydin, B. A. Pearlmutter, A. A. Radul, and J. M. Siskind, "Automatic differentiation in machine learning: A survey," *J. Mach. Learn. Res.*, vol. 18, pp. 1–43, Apr. 2018.

[36] C. Zhu, R. H. Byrd, P. Lu, and J. Nocedal, "Algorithm 778: L-BFGS-B: Fortran subroutines for large-scale bound-constrained optimization," *ACM Trans. Math. Softw.*, vol. 23, no. 4, pp. 550–560, 1997.

[37] M. E. Jerrell, "Automatic differentiation and interval arithmetic for estimation of disequilibrium models," *Comput. Econ.*, vol. 10, no. 3, pp. 295–316, 1997.

[38] G. F. Corliss, "Applications of differentiation arithmetic," in *Reliability in Computing*. Amsterdam, The Netherlands: Elsevier, 1988, pp. 127–148.

[39] D. B. Work, O.-P. Tossavainen, S. Blandin, A. M. Bayen, T. Iwuchukwu, and K. Tracton, "An ensemble Kalman filtering approach to highway traffic estimation using GPS enabled mobile devices," in *Proc. 47th IEEE Conf. Decis. Control*, 2008, pp. 5062–5068.

[40] M. J. Lighthill and G. B. Whitham, "On kinematic waves II. A theory of traffic flow on long crowded roads," *Proc. Roy. Soc. London. A. Math. Phys. Sci.*, vol. 229, no. 1178, pp. 317–345, 1955.

[41] P. I. Richards, "Shock waves on the highway," *Oper. Res.*, vol. 4, no. 1, pp. 42–51, 1956.

[42] A. Bressan, *Hyperbolic Systems of Conservation Laws: The One-Dimensional Cauchy Problem*, vol. 20. Oxford, U.K.: Oxford Univ. Press on Demand, 2000.

[43] S. N. Kružkov, "First order quasilinear equations in several independent variables," *Math. USSR-Sbornik*, vol. 10, no. 2, p. 217, 1970.

[44] R. J. LeVeque and R. J. Leveque, *Numerical Methods for Conservation Laws*, vol. 132. Basel, Switzerland: Springer, 1992.

[45] M. Treiber and A. Kesting, "Traffic flow dynamics," *Data, Models Simulation*. Berlin, Germany: Springer-Verlag, 2013.

[46] B. Greenshields et al., *A Study of Traffic Capacity*, Nat. Res. Council, Ottawa, ON, Canada, 1935.

[47] C. F. Daganzo and N. Geroliminis, "An analytical approximation for the macroscopic fundamental diagram of urban traffic," *Transp. Res. B Methodol.*, vol. 42, no. 9, pp. 771–781, 2008.

[48] F. L. Hall and L. M. Hall, "Capacity and speed-flow analysis of the queen Elizabeth way in Ontario," *Transp. Res. Rec.*, vol. 1990, no. 1287, pp. 108–118, 1990.

[49] A. Srivastava and N. Geroliminis, "Empirical observations of capacity drop in freeway merges with ramp control and integration in a first-order model," *Transp. Res. C Emerg. Technol.*, vol. 30, pp. 161–177, May 2013.

[50] F. L. Hall and K. Agyemang-Duah, "Freeway capacity drop and the definition of capacity," *Transp. Res. Rec.*, vol. 1991, no. 1320, pp. 1–8, 1991.

[51] M. Raissi, P. Perdikaris, and G. E. Karniadakis, "Physics informed deep learning (part I): Data-driven solutions of nonlinear partial differential equations," 2017, *arXiv:1711.10561*.

[52] M. Raissi, P. Perdikaris, and G. E. Karniadakis, "Physics informed deep learning (part II): Data-driven discovery of nonlinear partial differential equations," 2017, *arXiv:1711.10566*.

[53] J. Lebacque, "The Godunov scheme and what it means for RST order TRA C OW models," in *Proc. 13th Int. Symp. Transp. Traffic Theory*, vol. 2426. Lyon, France, Jul. 1996, p. 36.

[54] P.-E. Mazaré, A. H. Dehwah, C. G. Claudel, and A. M. Bayen, "Analytical and grid-free solutions to the Lighthill–Whitham–Richards traffic flow model," *Transp. Res. B Methodol.*, vol. 45, no. 10, pp. 1727–1748, 2011.

[55] L. Xue, Y. Yang, and D. Dong, "Roadside infrastructure planning scheme for the urban vehicular networks," *Transp. Res. Procedia*, vol. 25, no. 25, pp. 1380–1396, 2017.

[56] US Department of Transportation. "FHWA, 2008a. NGSIM—Next generation simulation." [Online]. Available: http://www.ngsim.fhwa.dot.gov/ (Accessed: May 24, 2021).

[57] X.-Y. Lu and A. Skabardonis, "Freeway traffic shockwave analysis: Exploring the NGSIM trajectory data," in *Proc. 86th Annu. Meeting Transp. Res. Board*, Washington, DC, USA, 2007, pp. 1–9.

[58] V. Alexiadis, J. Colyar, J. Halkias, R. Hranac, and G. McHale, "The next generation simulation program," *Inst. Transp. Eng. ITE J.*, vol. 74, no. 8, p. 22, 2004.

[59] H. Yeo and A. Skabardonis, "Parameter estimation for NGSIM over-saturated freeway flow algorithm," in *Proc. 10th AATT Conf.*, 2008, pp. 1–9.

[60] J. Liu, M. Barreau, M. Cicic, and K. H. Johansson, "Learning-based traffic state reconstruction using probe vehicles," 2020, *arXiv:2011.05031*.

[61] X. Ying, "An overview of overfitting and its solutions," *J. Phys. Conf.*, vol. 1168, no. 2, 2019, Art. no. 022022.

[62] B. Ghojogh and M. Crowley, "The theory behind overfitting, cross validation, regularization, bagging, and boosting: Tutorial," 2019, *arXiv:1905.12787*.

[63] G. Raskutti, M. J. Wainwright, and B. Yu, "Early stopping and non-parametric regression: An optimal data-dependent stopping rule," *J. Mach. Learn. Res.*, vol. 15, no. 1, pp. 335–366, 2014.

[64] M. Bramer, "Using J-pruning to reduce overfitting in classification trees," in *Research and Development in Intelligent Systems XVIII*. London, U.K.: Springer, 2002, pp. 25–38.

[65] Y. Sun, X. Wang, and X. Tang, "Deep learning face representation from predicting 10,000 classes," in *Proc. IEEE Conf. Comput. Vis. Pattern Recognit.*, 2014, pp. 1891–1898.

**ARCHIE J. HUANG** received the B.Eng. degree in electrical engineering from Tsinghua University, and the M.S. degree in applied urban science and informatics from New York University. He is currently pursuing the Ph.D. degree with the Civil, Environmental, and Construction Engineering Department, University of Central Florida. He was a Senior Researcher with the Electrical and Computer Engineering Department, California State University, Los Angeles. His research and working interests include traffic state estimation and deep learning.

**SHAURYA AGARWAL** (Senior Member, IEEE) received the B.Tech. degree in electronics and communication engineering from the Indian Institute of Technology Guwahati, and the Ph.D. degree in electrical engineering from the University of Nevada, Las Vegas in 2015. Since 2018, he has been an Assistant Professor with the Civil, Environmental, and Construction Engineering Department, University of Central Florida. He is the Founding Director of Urban Intelligence and Smart City (URBANITY) Lab. He was previously an Assistant Professor with the Electrical and Computer Engineering Department, California State University, Los Angeles, from 2016 to 2018. He completed his postdoctoral research with New York University in 2016. His research focuses on interdisciplinary areas of cyber–physical systems, smart and connected transportation, and connected and autonomous vehicles. Passionate about cross-disciplinary research, he integrates control theory, information science, data-driven techniques, and mathematical modeling in his work. As of May 2022, he has published one book, over 26 peer-reviewed journal publications, and multiple conference papers. His work has been funded by several private and government agencies. He serves as an Associate Editor for IEEE TRANSACTIONS ON INTELLIGENT TRANSPORTATION SYSTEMS.